NUMERICAL COMPUTATION OF THE X-15 WIND TUNNEL AND FLIGHT EXPERIMENTS: A VALIDATION AND VERIFICATION CASE STUDY

Bernd Wagner*, Michael Mifsud*, Jason Bennett* and Scott Shaw*
***School of Engineering, Cranfield University, United Kingdom.**

Keywords: *computational fluid dynamics, validation, verification*

Abstract

A verification and validation study of the IMPNS space-marching flow solver has been undertaken for a complete hypersonic air-vehicle configuration. A hierarchical approach was adopted in which the vehicle aerodynamics was decomposed and related flow phenomenon studied. Using this hierarchy bench mark solutions and laboratory experiments were identified that provide the basis of the verification and validation exercises. Detailed comparisons of iterative and grid converged IMPNS computations with benchmark solutions and wind tunnel measurements are presented. Computations of the X-15 wind tunnel and flight experiments are described and comparison is made with measured surface and off-surface pressure measurements and wind tunnel flow visualization observations that demonstrate the reliability and capability of the IMPNS flow solver for complex configurations.

1 Introduction

The past 10 years have seen remarkable advances in the development and application of computational tools to problems in external aerodynamics. Progress has largely been driven by the increased availability of affordable high-performance computing and the emergence of reliable bespoke and commercial-off-the-shelf software packages that are well suited to the flow problems faced by the aeronautical engineer.

While the tools and supporting infra-structure have matured, the general view of the role of CFD both for analysis and design has remained remarkably unchanged. This view considers that the purpose of a CFD analysis is to provide the most accurate solution possible. This emphasis on obtaining the 'right answer' has hindered the wider up-take of CFD particularly within the aerospace design community.

An alternate approach advocated by Roache [1] and Oberkampf [2] is to accept that CFD may not be able to provide the 'right answer' and instead directs effort towards understanding and characterizing the error and uncertainty associated with the computed results. Within this paradigm the purpose of CFD simulations is not to produce solutions as accurately as possible, but instead provide solutions within an acceptable accuracy bound.

This change of philosophy is key to enhancing productivity and unlocking the capability of CFD to inform the design process.

In order to establish and characterize error uncertainty we require some knowledge of the 'right answer'. Identifying what is meant by the 'right answer' is difficult, but raises a number of important and fundamental issues.

The purpose of any computational simulation is to predict the behavior of a physical system and so at the most fundamental level the reliability of the simulation can be tested by comparing with the physical reality. However, real world experimental measurements are themselves subject to error and uncertainty and so may not provide a reliable basis for comparison. Instead we can consider comparison with laboratory experiments which offer a more controllable environment but may introduce new sources of error and are in

themselves models of the physical reality. Provided that experimental error and uncertainty is quantified and understood then we may use statistical techniques to help make meaningful comparisons between the experimental and computed data.

Alternatively we can ignore the physical basis of the model equations and instead consider the problem from a purely mathematical perspective. The computational simulation is a solution of an approximation to the physical reality and so we could suggest that it is the exact solution of the model equations that is the 'right answer', although the exact solution may not reproduce the physical reality upon which the governing equations are based. Unfortunately the exact solution is usually unknown, at least for physically meaningful cases. We must also recognize that the numerical solution of the finite difference equations is not in itself an exact solution of the governing partial differential equations due to the presence of truncation errors in the spatial and temporal discretization, errors in the specification of the initial and boundary conditions and errors related to the finite precision of the computer hardware upon which the computations are performed. Fortunately, using the mathematical concepts of consistency, stability and convergence we can demonstrate that in the limit $\Delta x \rightarrow 0$ and $\Delta t \rightarrow 0$ the numerical solution of the discretized equations should tend towards the exact solution of the partial differential equations upon which they are based and this can be used to develop strategies and approximations to the continuum solution.

Recognition that we may have more than one concept of the 'right answer' has led to the development of two specific approaches for formally assessing solution accuracy; verification and validation. Verification is a process that can be followed to demonstrate and understand the extent to which the governing equations are satisfied by the numerical solution while validation provides a measure of how well the mathematical model approximates the physical reality. It is important that a calculation is verified before it is used as the basis of a validation study.

In this paper we employ the verification and validation ideas of Roache [1] and Oberkampf et al [2,3] to perform an assessment of the reliability of Cranfield University's IMPNS flow solver. Computations are performed for a series of simple flows that isolate individual aspects of the expected flow physics. For these problems analytical and semi-analytical benchmark solutions are available that provide the basis of a verification study. More complex flows involving coupled physical phenomenon are addressed using comparisons with laboratory experiments. Having demonstrated the credibility of the IMPNS flow solver computations are then performed for the X-15 flight vehicle. Comparison is made with surface and off-surface pressure measurements and experimental observations made during wind tunnel and flight testing of the aircraft.

2 Flow Solver Details

The computations performed in the current study were undertaken using Cranfield University's IMPNS flow solver [3-10]. IMPNS has been developed to provide a rapid, robust and accurate solver for problems in high-speed external aerodynamics.

2.1 Governing Equations

IMPNS provides algorithms for the solution of the steady Euler, Thin-layer or Parabolized Navier Stokes equations together with appropriate turbulence closures. These equations are formulated for a finite control volume fixed in space resulting in a system of equations that can be written in the following conservative integral form,

$$\int_S \mathbf{F}_n \, dS = \mathbf{0} \qquad (1)$$

in which $\mathbf{F}_n$ is the flux through the surface of an arbitrary control volume bounded by the surface S. The governing equations are solved using an implicit space marching procedure that employs the approximate Riemann solver of Osher and

Solomon [11] for the discretization of the convective terms and a central difference based scheme for the viscous terms.

For flows in which there is no upstream influence a single sweep is employed starting at the nose of the configuration and proceeding in the stream wise direction. The approach has been extended to allow for flows with upstream influence, for example blunt body flows and flows exhibiting axial separation. In this case a multi-sweep procedure in which the solver marches backwards and forwards is employed to capture the elliptical characteristics of the governing equations.

2.2 Pseudo-Time Relaxation

The spatial discretization described in the preceding section results in a system of linear equations at each stream-wise marching plane that must be solved in order for the calculation to proceed.

This system is solved using a relaxation approach in which an additional pseudo-time derivative is added to the steady governing equations.

$$\frac{\partial}{\partial t}\int_V Q dV + \int_S \mathbf{F}_n dS = \mathbf{0} \qquad (2)$$

The implicit system is then solved by marching to the steady state in pseudo-time. The system is judged to have converged to the steady state once the normalized residual has fallen below a user specified value. This value is problem dependent and it is important that iterative convergence is demonstrated for each individual calculation.

Convergence of the pseudo time relaxation is accelerated through the use of a combination of an implicit Newton-Krylov method [12] and full multi-grid [13].

2.3 Turbulence Closure

A range of turbulence closures are available that include the algebraic models of Baldwin and Lomax [14] and Degani and Schiff [15], variants of the one-equation model of Spalart and Allmaras [16] and variants of Wilcox's two-equation k-w model [17]. The turbulence closure is coupled with the mean flow equations in a segregated fashion.

2.4 Grid Generation

IMPNS employs structured multi-block grids. To provide geometric flexibility and to reduce computational expense non-matching block faces are permitted in the stream-wise direction. This allows changes of grid topology in the stream wise direction, allowing the grid to better reflect the geometric characteristics of the configuration being studied.

3 The X-15 Test Programme

The X-15 was the worlds first manned hypersonic research aircraft setting a series of speed records in the Mach 4-6 range between 1959 and 1967 [18]. Uniquely, the aircraft was extensively instrumented providing a wealth of data on supersonic and hypersonic air flows, aerodynamic heating and stability and control. The geometric complexity of the aircraft coupled with the availability of extensive flight and wind tunnel test data provide an ideal opportunity to demonstrate credible, rapid CFD.

Fig. 1. X-15 Flight Research Vehicle.

A CAD database of the X-15 based upon original blue print documents in NASA's archive was provided by the Geometry Laboratory of the NASA Langley Research

Center [19]. The geometry was provided in two basic forms; a direct rendering of the engineering drawings and a watertight model that incorporates some additional simplifications intended for use by the CFD community. The latter model was employed in the present study. A rendering of the CAD database is presented in Fig. 2.

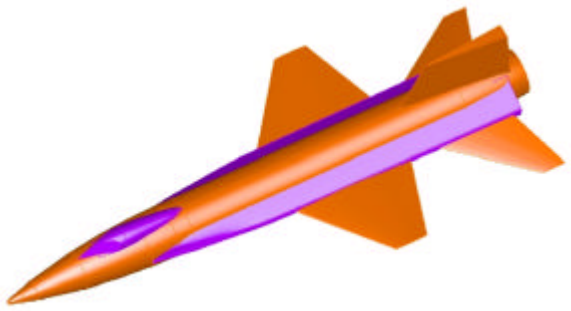

Fig. 2. Rendering of X-15 CAD Database [19]

4 Validation Hierarchy

It is impossible to demonstrate the validity of a computational model over its full range of applicability in any mathematically meaningful way. Instead we rely on empirical proofs. Clearly proof by exhaustion is impractical, indeed many have used this to argue that computational experiments can only provide the means to invalidate a model rather than validate it. Instead the process of validation relies on proof by induction in which the base case is validated and we rely on physical inference to prove the validity of the model for the parameter and configuration spaces that we wish to study.

The process of validation is therefore one of building a robust case, through collection of empirical evidence, to demonstrate the credibility of the simulation.

The construction of an evidential database is expensive, and may be impractical within the time constraints of a given project. Instead we advocate the use of an application based hierarchical approach in which the physical system is decomposed into successively simpler flow problems [3]. At the bottom of this hierarchy are component cases that exhibit isolated physical phenomena, for example a shock wave or a boundary layer. As the hierarchy is traversed the cases increase in physical and geometric complexity until the full complexity of the desired application is reached. The validation hierarchy used in the current work is illustrated in Fig. 3.

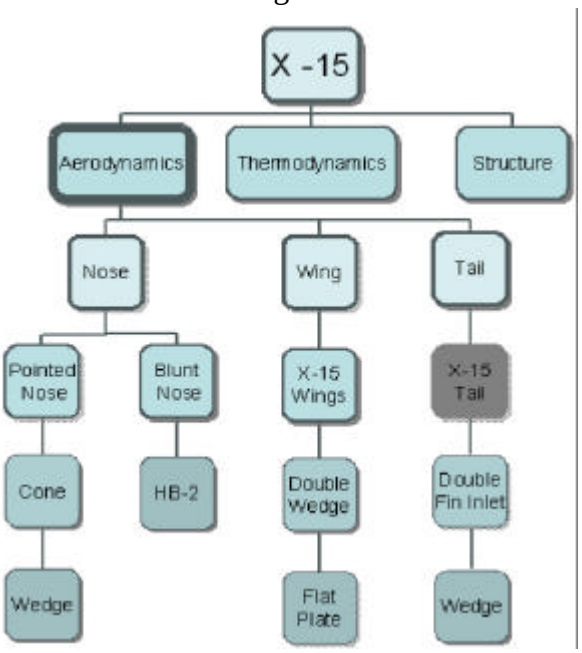

Fig. 3. X-15 Validation Hierarchy

5 Verification and Validation

Verification studies were undertaken for several cases for which analytical or semi-analytical results are known; see for example Mifsud and Shaw [20] and Wagner [21]. These test problems typically concern isolated physical phenomena, such as a shock-wave or a boundary layer, and simple geometry and correspond to the lowest level of the hierarchy. In this paper we consider a single example, the inviscid flow over a compression corner to illustrate our approach to verification.

Several related validation studies [20,21] were also undertaken that involved complex geometry and multiple physical phenomena. Efforts were made to compare IMPNS computations with good quality experimental data and independent simulations whenever possible. The validation cases typically represent the middle and higher levels of the validation hierarchy. In this paper we present a

single case, the supersonic turbulent flow over an ogive fore-body.

5.1 Compression Corner

This verification test case involves the study of inviscid flow over a 15° compression corner at a Mach number of 2.5. Extensive iterative and grid convergence studies were undertaken before data was compared with the theoretical result. The finest grid considered contained approximately 80,000 nodes. The main results are summarised in Table 1, while a visualization of the computed flow is shown in Fig. 4. The visualization shows the expected result, two regions of uniform flow separated by a discontinuity. In the present computations the shock is relatively thick, no effort has been made to align species of grid lines with the flow features. This leads to numerical artefacts, non uniform pressure and temperature, in the solution near the solid surface. These artefacts can be eliminated by improving shock resolution or by starting the simulation downstream of the leading edge.

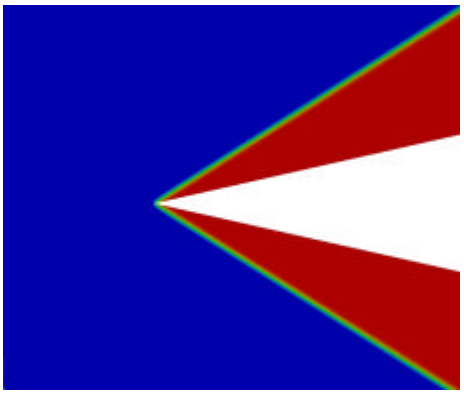

Fig. 4. Computed flow over compression corner

Physical Property	Theory	IMPNS
Local Mach Number	1.8735	1.8737
Pressure Ratio	2.4675	2.4676
Density Ratio	1.8665	1.8668
Temperature Ratio	1.3220	1.3218
Axial Force	0.0899	0.0899
Normal Force	-0.3354	-0.3354

Table 1. Comparison of computed and theoretical results, compression surface

The computed pressure forces acting along the surface of the compression corner were extrapolated to the continuum solution using the method based upon Richardson extrapolation suggested by Roache [1]. Agreement with the exact and extrapolated solutions is considered to be excellent.

5.2 RAE B1A Ogive Fore-body

This validation case involves the computation of the flow over the RAE B1A [22,23] tangent-ogive fore-body. The RAE B1A ogive-cylinder body geometry consists of a 3 calibre ogive nose having a cubic profile followed by a 10 calibre cylinder of 3.7 inches diameter. Comparisons are made at a Mach number of M = 2.5, a Reynolds number based on diameter of 1,123,100 and an incidence of 14 degrees.

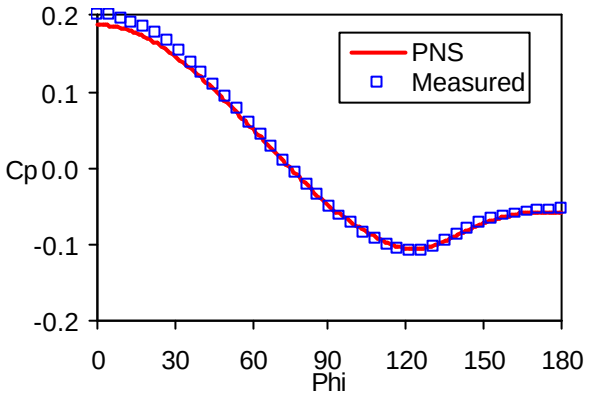

(a) x/D = 2.4

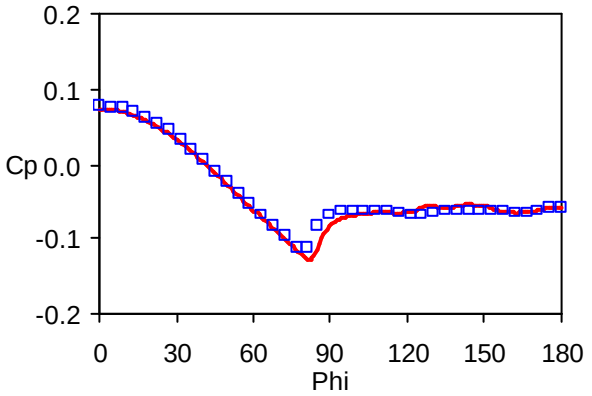

(b) x/D = 9.5

Fig. 5. Comparison of computed and measured pressure distributions, DERA B1A

Extensive iterative and grid convergence studies were undertaken. The finest grid for which IMPNS computations are presented involved approximately 5.275 million cells. Comparisons of the computed and measured pressure distributions at two axial stations are presented in Fig. 5. Agreement between the computed and measured data is good.

The computed and measured force and moment coefficients are presented in Table 2. Agreement with the wind tunnel measurements is generally good, the predictions of normal force, pitching moment and centre of pressure are within 1-2%. Axial force is less well predicted with an error of approximately 6%. Assessment of the discretization error using the approach suggested by Roache [1] indicates that the discretization error associated with the fine grid computations is at worst ±0.6%.

	IMPNS	Measured
C_A	0.199	0.186
C_N	1.88	1.91
C_m	-10.13	-10.24
X_{cp}	5.39	5.36

Table 2. Comparison of computed and measured force and moment coefficients for the RAE B1A

In validating our results we have also tried to make use of independent computations whenever possible. This serves as verification of our model implementation when the model is of similar fidelity and validation when the model is of higher-fidelity. In this respect the B1A fore-body is a good example as the experimental dataset has formed the basis of several multi-national CFD validation exercises. Comparison of the present computations of normal and pitching moment coefficient with those of Grove and Wang [24] is made in Table 3. The data of Grove and Wang were selected due to the range of modeling options investigated and the fact that the COBALT computations were performed in conjunction with a tree-based Cartesian grid adaptation procedure and so are likely to be grid converged. The present computations are in excellent overall agreement. Grove and Wang do not report the axial force coefficient obtained in their computations.

Computation	Cy	Cm
IMPNS SA	1.88	-10.13
COBALT DES-SST[15]	1.90	-10.33
COBALT DES-SA[15]	1.89	-10.21
COBALT SA[15]	1.89	-10.23
COBALT SST[15]	1.90	-10.33
COBALT KW[15]	1.90	-10.32

Table 3. Comparison of IMPNS and Cobalt Computations, DERA B1A fore-body

6 X-15 Results

Having established the reliability of the IMPNS solver for isolated and coupled flow phenomena of interest computations were then performed for the X-15 research aircraft.

Initially computations were performed for the nose geometries investigated by Franklin [25]. Two configurations were computed; a sharp nose geometry for which single sweep computations were performed and a geometry with a spherically blunted nose for which multi-sweep computations were required. The computations were performed for a Mach number of $M_\infty = 4.7$, an incidence of $\alpha = 0°$ and a Reynolds number of 10,500,000 per metre. Comparisons of the computed and sub-scale wind tunnel pitot pressure survey data at two axial locations (x/L = 0.045 and x/L = 0.1246) are presented in Fig. 6 for the blunt nose configuration.

Agreement between the computations and experiment is generally good close to the fuselage surface. Further away agreement is poor although the location of the shock is well captured. The present computations agree well with those presented by Hawkins and Dilley [31].

The corresponding Mach number profile is shown in Fig. 7. The agreement between the computed and measured Mach number profile is much improved. This is surprising, as the measured data is based upon the pitot pressure measurements of Fig. 6. It is thought that the

pitot pressure data presented in Fig. 6 has been evaluated inappropriately. This will be investigated further in future work.

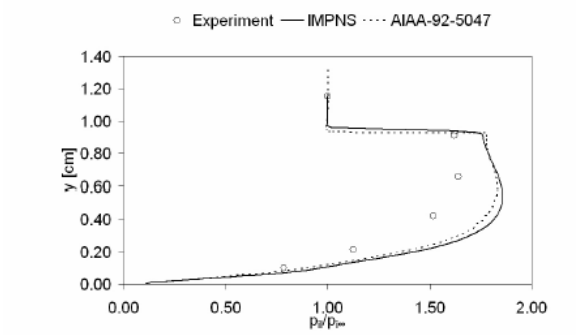

(a) x/L = 0.045

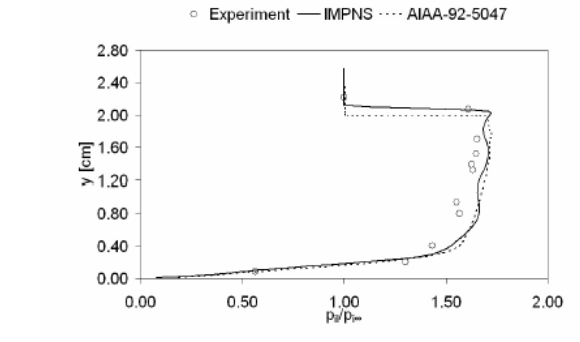

(b) x/L = 0.1246

Fig. 6. Comparison of computed and measured pitot pressures for the blunt nose configuration

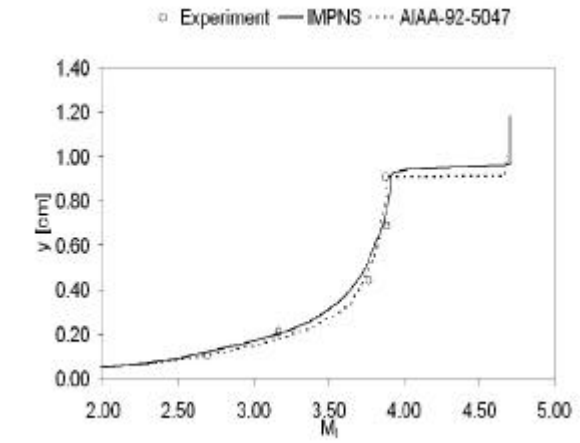

(a) x/L = 0.045

Fig. 7. Comparison of computed and measured Mach number for the blunt nose configuration

Fig.8 presents comparisons of measured and computed surface pressure coefficients at several stations further along the fuselage, x/L = 0.223, in the region of the cock-pit, x/L = 0.297 and fuel tank fairing x/L = 0.501. In these figures data are presented for both 0° and 15° incidence. Agreement between the computations and experimental data is acceptable.

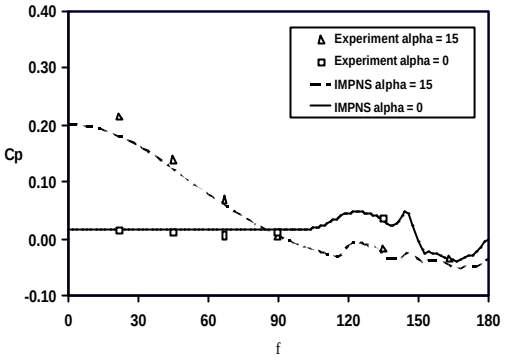

(a)x/L = 0.223

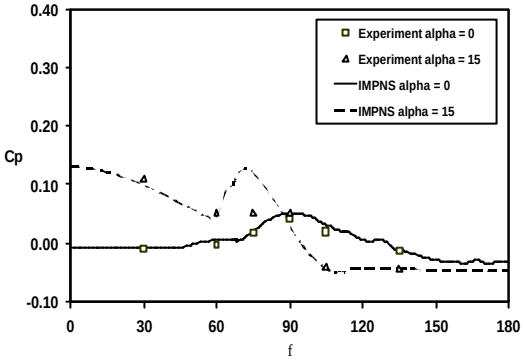

(b) x/L = 0.297

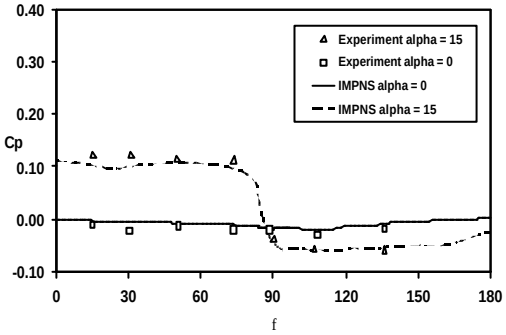

(c) x/L = 0.501

Fig. 8. Comparison of surface pressures for the blunt nose configuration.

Computations for the X-15 flight experiment were also performed at a Mach number of $M_\infty = 4.7$, at incidences of $\alpha = 0°$ and $\alpha = 15°$ and a Reynolds number of 2,900,500

per metre. The flow was assumed to be fully turbulent. Fig. 9 compares the measured and computed surface pressure distributions at x/L = 0.0337. The agreement is considered to be excellent considering the uncertainties when matching the flight condition. As with the wind tunnel experiments the surface pressure distribution along the forebody is in better agreement with the measured data than the off surface data, Fig. 10.

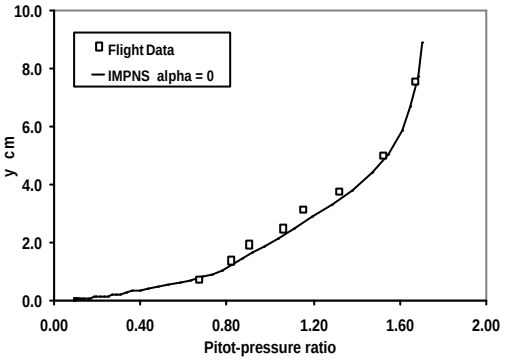

Fig. 9. Comparison of off surface pressures for the flight test configuration x/L = 0.0337.

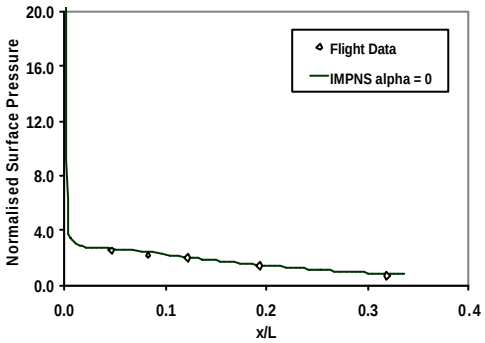

Fig. 10. Comparison of surface pressures for the flight test configuration.

The final comparisons of the current work are presented for the flow over the wings. Fig. 11 shows computed and measured surface pressure coefficient data at the mid-span location. The agreement is good. Fig. 12., which compares the observed and computed shock location for the 15° incidence case, suggests that the mid-span location lies within the region influenced by the nose, but is outside of that influenced by the weaker fairing shock. The observed shock locations are in excellent agreement with those observed in the wind tunnel experiment.

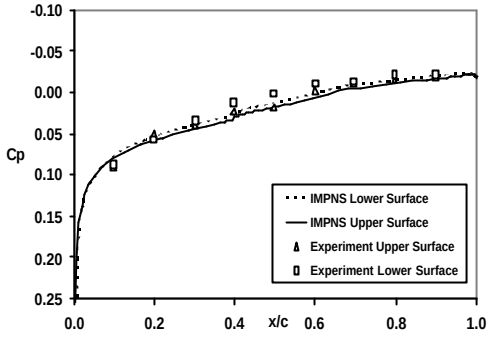

(a) $\alpha = 0°$

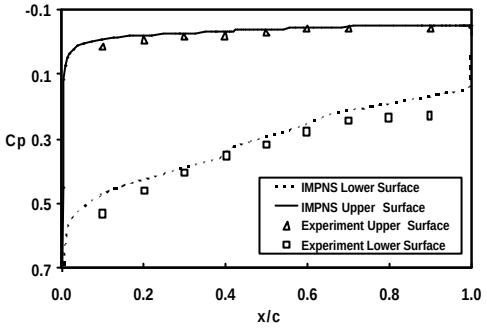

(b) $\alpha = 15°$

Fig. 11. Comparison of measured and computed surface pressure distributions over the wing

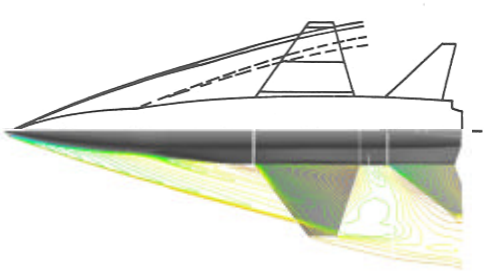

Fig. 12. Comparison of Computed and Observed Shock Structure

7 Conclusions

An extensive verification and validation study of Cranfield University's IMPNS flow solver has been performed for a complete hypersonic air-vehicle configuration. A hierarchical approach was adopted in which the vehicle

aerodynamics were decomposed using vehicle sub-systems and related flow phenomenon. Using this hierarchy bench mark solutions and laboratory experiments were identified that provide the basis of the verification and validation exercises. Detailed comparisons of iterative and grid converged IMPNS computations with benchmark solutions and wind tunnel measurements are presented.

Verification computations demonstrating the capability of the IMPNS solver for flows involving isolated shock waves, rarefaction fans and boundary layers were presented. Comparison was made with a range of benchmark solutions including analytical solutions of the governing equations, closed-form solutions of related ordinary differential equations and numerical solutions of related ordinary differential equations. Comparison between the computed data and benchmark solutions was generally excellent.

Validation computations were performed for flows that exhibit coupling of two or more of the isolated physical phenomena. For these cases comparison was made with well documented wind tunnel laboratory experiments. In addition to flows related to the verification study computations were also performed for a detached shock wave. Agreement between the IMPNS computations and the experimental data was generally good.

Finally computations of the X-15 flight experiment were performed and comparison was made with measured surface static pressures and off surface pitot pressure measurements. The comparisons demonstrate the reliability and capability of the IMPNS flow solver for complex configurations.

Acknowledgments

Bernd Wagner was supported under the EU ERASMUS programme. Michael Mifsud was supported by a CASE award funded jointly by EPSRC and DSTL. Jason Bennett was supported by a CASE award funded jointly by EPSRC and QinetiQ Ltd.

The authors are grateful to Trevor Birch (DSTL) for his enthusiastic support of the IMPNS development and his help in obtaining experimental data and the X-15 CAD database.

The authors would also like to thank NASA Langley's Geolab for making their geometric model of the X-15 flight vehicle available for use in the current study.

References

[1] Roache, PJ. Verification and Validation in Computational Science and Engineering, Hermosa Publishers, 1998.

[2] Oberkampf, WL and Blottner, FG. Issues in Computational Fluid Dynamics Code Verification and Validation, AIAA Journal, Vol. 36, No. 5, pp. 687-695, 1998.

[3] Oberkampf, WL, Trucano, TG. Verification and validation in computational fluid dynamics, Progress in Aerospace Sciences, Vol. 38 (3), pp. 209-272, 2002.

[4] Qin N and Richards BE. Finite volume 3DNS and PNS solutions of hypersonic viscous flows around a delta wing using Osher's flux difference splitting, Proc. of a Workshop on Hypersonic Flows for Re-entry Problems, 1990.

[5] Birch TJ, Qin N and Jin X. Computation of supersonic viscous flows around a slender body at incidence, AIAA Paper 94-1938, 1994.

[6] Shaw ST and Qin N. A matrix-free preconditioned Krylov subspace method for the PNS equations, AIAA Paper 98-111, 1998.

[7] Qin N, Ludlow DK, Zhong B, Shaw ST and Birch TJ. Multi-grid acceleration of a preconditioned GMRES implicit PNS solver, AIAA Paper 99-0779, 1999.

[8] Birch TJ, Ludlow DK and Qin N. Towards an efficient, robust and accurate solver for supersonic viscous flows, Proc. of the ICAS 2000 Congress, Harrogate, UK, 2000.

[9] Birch TJ, Prince SA, Ludlow DK and Qin N. 'The application of a parabolized Navier-Stokes solver to some hypersonic flow problems', AIAA Paper 2001-1753, 2001.

[10] Qin N and Ludlow DK. A cure for anomalies of Osher and AUSM+ schemes for hypersonic viscous flows around swept cylinders, Proc. of the 22nd International Symposium on Shock Waves, Imperial College, London, UK, July 18-23, (Editors: Ball GJ, Hillier R and Roberts GT), pp. 635-640, 1999.

[11] Osher S and Solomon F. Upwind Difference Schemes for Hyperbolic Systems of Conservative Laws, Math. of Comp. 38, 339–374, 1992.

[12] Saad Y and Schultz MH. GMRES: A generalised minimal residual algorithm for solving non-symmetric linear systems, SIAM J. Sci. Stat. Comput. 7, pp. 856–869, 1986.

[13] Brandt A. Multi-Level Adaptive Solutions to Boundary-Value Problems, Math. of Comp. 31, pp. 333–390, 1977.

[14] Baldwin B and Lomax H. Thin-layer approximation and algebraic model for separated turbulent flows, AIAA 16th Aerospace Sciences Meeting, Huntsville, AL, Jan. 16–18, 1978.

[15] Degani D and Schiff LB. Computation of Turbulent Supersonic Flows around Pointed Bodies Having Crossflow Separation, J. Comp. Phys. 66, pp. 173–196, 1986.

[16] Spalart PR and Allmaras SR. A one-equation turbulence model for aerodynamic flows, AIAA Paper 92-0439, 1992.

[17] Wilcox, DC. Turbulence Modeling for CFD Second Edition, DCW Industries, 1998.

[18] Stillwell WH. X-15 research results - with a selected bibliography, NASA SP-60. NASA, Washington, D.C., 1965.

[19] Birch, TJ. Private Communication, 2005.

[20] Mifsud, M and Shaw ST. Credible simulations of supersonic weapon configurations using the IMPNS flow solver, IMPNS-Report 2005-2, Cranfield University, 2005.

[21] Wagner, BH. PNS Computations of configurations related to realistic space vehicles, M.Sc. Thesis, Cranfield University, 2005.

[22] Hodges, J Ward, LC and Birch, TJ. Pressure Measurements on Slender Bodies at Supersonic Speeds and Development of Flow Separation Criteria for Euler Codes, RAE TM Aero 2177, 1990.

[23] Ward, LC and Birch, TJ. An Investigation of Reynolds Number Effects on a Tangent-Ogive Cylinder Body, DRA TM Aero/Prop 4, 1992.

[24] Grove, DV Wang, ZJ. Computational Fluid Dynamics Study of Turbulence Modeling for an Ogive using Cobalt flow solver and a 2n Tree-Based Cartesian Grid Generator, AIAA 2005-1042, 2005.

[25] Franklin AE and Lust RM. Investigation of the aerodynamic characteristic of a 0.067-scale model of the X-15 airplane (configuration 3) at Mach numbers of 2.29, 2.98 and 4.65, NASA TM X-38, Washington, D.C., 1959.

[26] Palitz M Measured and calculated flow conditions on the forward fuselage of the X-15 airplane and model at mach numbers from 3.0 to 8.0, NASA TN D-3447, Washington, D.C., 1966.

[27] Hodge L and Burbank PB. Pressure distribution of a 0.0667-scale model of the X-15 airplane for an angle-of-attack range of 0 to 28 at Mach number of 2.30, 2.88 and 4.65, NASA TM X-275, Washington, D.C., 1960.

[28] Silvers, HN, Lancaster, JA amd Wills, JS. Investigation of the loading characteristics of the lifting surfaces and the speed brakes of a 0.067 scale model of the North American X-15 airplane (configuration 3) at Mach numbers of 2.29, 2.98 and 4.65, NASA TM X-301, 1960.

[29] Pyze, JS. Flight-measured wing surface pressures and loads fot the X-15 airplane ay Mach numbers from 1.2 to 6, NASA TN D-2602, 1965.

[30] Keener, ER and Pembo, C. Aerodynamics forces on components of the X-15 airplane, NASA TM X-712, 1961.

[31] Hawkins R and Dilley A. CFD comparisons with wind tunnel and flight data for the X-15., In *AIAA 4th International Aerospace Planes Conference*, AIAA 92-5047, Orlando, US-FL, 1992.